ELSEVIER

Physica C 340 (2000) 33–40

PHYSICA C

www.elsevier.nl/locate/physc

An all-sputtered buffer layer architecture for high-J_c $YBa_2Cu_3O_{7-\delta}$ coated conductors

T. Aytug [a,b,*], J.Z. Wu [a], B.W. Kang [b], D.T. Verebelyi [b], C. Cantoni [b], E.D. Specht [b], A. Goyal [b], M. Paranthaman [b], D.K. Christen [b]

[a] *Department of Physics and Astronomy, University of Kansas, Lawrence, KS 66045, USA*

[b] *Oak Ridge National Laboratory, Building 3115, MS-6061, Bethel Valley Road, P.O. Box 2008, Oak Ridge, TN 37831-6061, USA*

Received 3 March 2000; received in revised form 6 June 2000; accepted 8 June 2000

Abstract

We report the development of an all-sputter-deposited buffer multilayer architecture for the growth of high critical current density (J_c) $YBa_2Cu_3O_{7-\delta}$ (YBCO) films on metallic tapes. The structure comprises the layer sequence of CeO_2/YSZ/LNO (YSZ: yttria stabilized zirconia, LNO: $LaNiO_3$) on biaxially textured Ni substrates. X-ray diffraction analysis of the base $LaNiO_3$ (LNO) layers indicated that well textured films can be obtained at deposition temperatures (T_{dep}) between 450°C and 500°C, while higher T_{dep} yielded polycrystalline films. The degree of LNO crystallinity was also influenced by the oxygen partial pressure during the growth. Scanning electron microscopy observations revealed a smooth, dense and crack-free surface morphology, independent of film thickness in the range of 50–300 nm. Subsequent YSZ and CeO_2 films were deposited to complete the buffer-layer structure. Epitaxial YBCO films grown by pulsed laser ablation on the CeO_2/YSZ/LNO/Ni multilayer structure have self-field J_c values as high as 1.3×10^6 A/cm^2 at 77 K. Effects of the LNO base-layer thickness on the quality of buffers and on the superconducting properties of YBCO films showed no remarkable differences. The present results demonstrate a viable approach for the production of long length YBCO superconducting wires. © 2000 Elsevier Science B.V. All rights reserved.

PACS: 74.72.Gr; 74.76.Bz

Keywords: High-temperature superconductors; $YBa_2Cu_3O_{7-\delta}$; $LaNiO_3$; Sputtering; Buffer layers

1. Introduction

The recent development of rolling-assisted biaxially textured substrates (RABITS) offers promise for the fabrication of $YBa_2Cu_3O_{7-\delta}$ (YBCO)-based coated conductors [1,2], supporting high current for electric utility and high magnetic field applications at 77 K. A key issue in the RABITS approach is the necessity to use buffer layer structures that are compatible with both the underlying metal substrate, Ni or Ni-alloy, and the top superconducting YBCO layer. The function of the buffer layer is two fold. It prevents diffusion of Ni into the superconductor during high-temperature processing, and also transfers the biaxial texture of the metal substrate to the high temperature

* Corresponding author. Present address: Oak Ridge National Laboratory, Building 3115, MS-6061, Bethel Valley Road, P.O. Box 2008, Oak Ridge, TN 37831-6061, USA. Tel.: +1-865-574-6271; fax: +1-865-574-6263.

E-mail address: aytug@solid.ssd.ornl.gov (T. Aytug).

0921-4534/00/$ - see front matter © 2000 Elsevier Science B.V. All rights reserved.
PII: S0921-4534(00)01331-9

superconducting (HTS) coating. To date, studies have concentrated mainly on the buffer-layer combination of CeO_2 and yttria stabilized zirconia (YSZ), and high-quality YBCO films have been grown on RABITS with a layer sequence of YBCO/CeO_2/YSZ/CeO_2/Ni [2–6]. In this architecture, oxide buffer layers were grown either exclusively by pulsed laser deposition (PLD) or by a combination of electron beam evaporation (e-beam) and r.f. magnetron sputtering. Although techniques to grow epitaxial oxide buffer layers exclusively by sputtering on Ni tapes have been demonstrated [7], YBCO films with high superconducting critical current density (J_c) had not been achieved on these all-sputter buffered Ni tapes. The principal problem with an all-sputtered buffer architecture is the attainment of reproducible epitaxy in the base-CeO_2 layer on Ni.

A major challenge in utilizing any of these buffer-deposition techniques is prevention of unfavorably oriented NiO on the Ni surface. This requirement is difficult in principle, since epitaxial growth of oxide films generally requires elevated temperatures and oxidizing environments. To overcome this oxidation problem, buffer-layer growth is usually conducted under conditions that reduce NiO [2–8], but adequately oxidize buffer film. In addition to the Ni oxidation problem, an issue of concern has been the formation of cracks in the base-CeO_2 layer at thicknesses greater than a few hundred angstroms [3,9,10]. It is well understood that integrity of a base-buffer layer is extremely important for the epitaxial growth of subsequent oxide buffer and HTS layers. To overcome these problems, it is important and desirable to develop an alternative buffer layer architecture, that has a more adaptive and robust base-buffer layer and may be deposited in a more flexible fabrication scheme. Ideally, a single, scalable deposition technique for the growth of all buffer layers is preferred to minimize the difficulties and the cost of process scaleup. From practical considerations of mechanical simplicity and performance, sputtering serves as a scalable and versatile method for the growth of epitaxial oxide films.

$LaNiO_3$ (LNO) is a NiO-based compound with a perovskite crystal structure. The pseudocubic lattice parameter of 0.385 nm is a close match to that of the YBCO basal plane. Previously, He et al. reported sputter deposition of highly textured LNO buffer layers directly on Ni tapes [11]. However, YBCO films deposited directly on these LNO buffers showed depressed superconducting critical temperatures (T_c) of 75–80 K, due to diffusion of Ni into the YBCO lattice. Nevertheless, that work pointed to the potential viability of LNO as a base-buffer layer on Ni, and the possibility of an all-sputtered buffer architecture. Here, we report the successful fabrication of high-J_c YBCO coatings on an all-sputtered buffer architecture for the first time, employing the layer sequence CeO_2/YSZ/LNO/Ni.

2. Experimental

Biaxially textured Ni substrates were obtained from randomly oriented high purity (99.99%) Ni bars, which were first mechanically deformed by cold-rolling and then annealed in vacuum at 1000°C for 1 h, to obtain the desired (1 0 0) cube texture. Buffer layer depositions were performed with a r.f. magnetron sputtering system of base pressure 1×10^{-6} Torr, using oxide sputter targets that were 95 mm in diameter. Unlike the sintered and hard-pressed CeO_2 and YSZ targets, the LNO target was made from a single-phase LNO powder, which was lightly packed into a copper tray. Biaxially textured Ni substrates were mounted with conductive silver paste onto a heated substrate block assembly, in an on-axis sputter geometry. Deposition of LNO base layers was accomplished at substrate temperatures (T_{dep}) ranging from 400°C to 550°C. In order to suppress the formation of NiO, a reducing forming gas (96% Ar + 4% H_2) was used at the initial stages of LNO growth (≈2–3 min), followed by deposition in oxidizing conditions at a total pressure of 10 mTorr. During this stage, the partial pressure of O_2 (P_{O_2}) was varied in the range of 0.1–1 mTorr to observe the effect of O_2 on the growth of LNO layers. The deposition rate was ≈0.42 Å/s. The LNO film thickness was varied in the range of 50–300 nm, to investigate the effect on the microstructure and on the superconducting properties of the subsequent buffer and HTS layers, respectively.

Epitaxial YSZ layers were deposited on LNO/Ni substrates in an oxidizing environment. Typical sputtering conditions consisted of a mixture of forming gas and O_2 at a pressure ratio of $P(O_2)/P(96\%\ Ar + 4\%\ H_2) = 5\%$, with a total pressure of 10 mTorr and a substrate temperature in the range of 600–650°C. The deposition rate was ≈0.28 Å/s, with a corresponding film thickness of about 500 nm. Deposition of the top CeO_2 layers were accomplished in 10 mTorr of forming gas at a substrate temperature of 650°C. Typical thickness of the CeO_2 layer was 30 nm.

The PLD technique was employed for deposition of the YBCO films, using a XeCl excimer laser system, operated with an energy density of ≈4 J/cm^2. During deposition of the YBCO films, the substrates were kept at 780°C in 120 mTorr of O_2. After deposition, the samples were first cooled to 600°C at a rate of 5°C/min; then the O_2 pressure was increased to 550 Torr, and the samples cooled to room temperature at the same rate. Typical film thicknesses of YBCO coatings were 200 nm. Film crystal structures were characterized with a Huber high-resolution X-ray diffractometer (XRD), and microstructural analyses were conducted on a JOEL model, JSM-840 scanning electron microscope (SEM). A standard four-probe technique was used to evaluate the electrical properties of the samples. Electrical contacts of silver were deposited onto the samples using d.c. magnetron sputtering followed by an O_2 annealing in 1 atm for 30 min at 500°C. Values of J_c were assigned at a 1 μV/cm criterion.

3. Results and discussion

3.1. Growth of $LaNiO_3$ base layers on biaxially textured Ni substrates

Fig. 1 shows the XRD θ–2θ spectrum for a series of LNO films deposited at various temperatures ranging from 400°C to 550°C at a fixed $P_{O_2} = 0.5$ mTorr. At $T_{dep} \leqslant 450$°C, broad (0 0 l) reflections from LNO films are evidence of inhomogeneity or high defect density. For 450°C < T_{dep} < 550°C, reflections are sharper, indicating more perfect films. Above 500°C, however, the

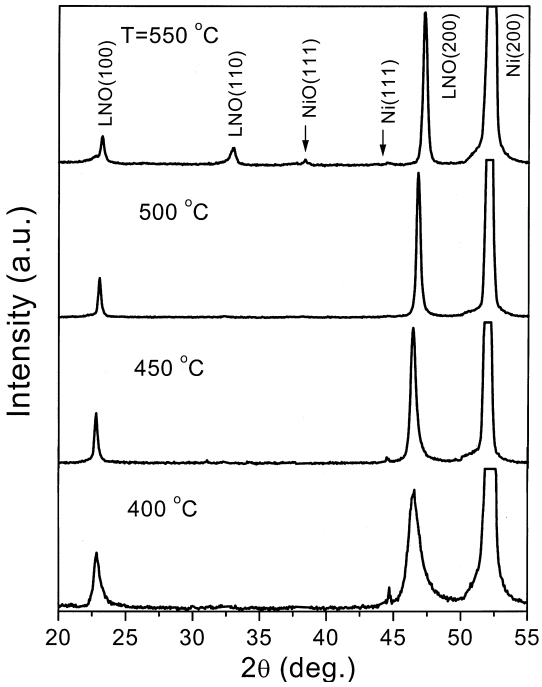

Fig. 1. XRD θ–2θ patterns of LNO films grown on biaxially textured Ni substrates at various substrate temperatures.

films showed extra LNO (1 1 0) and NiO (1 1 1) components along with the LNO (0 0 l) reflections, indicating that the single crystalline orientation of the films gradually changed to polycrystalline. This observed growth behavior of LNO at elevated temperatures (T_{dep} > 500°C) may be attributed to the formation of (1 1 1) textured NiO layer on the surface of the Ni. The effect of T_{dep} on the in-plane (ϕ-scan) and the out-of-plane (ω-rocking curve) texture of LNO layers was also studied and the results are shown in Fig. 2(a) and (b), respectively. Note that biaxially textured Ni substrates generally have slightly different in-plane and out-of-plane textures depending on the specific rolling and crystallization conditions. Thus, to make a direct and more quantitative comparison between the deposition parameters and the crystalline quality of the grown films, the FWHM peak-width ratios relative to the underlying Ni is plotted as a function of T_{dep}. Considerable improvement in the in-plane and out-of-plane alignment of the LNO layers is observed with an increase in temperature above 400°C. Depositions at $T_{dep} \geqslant 450$°C did not

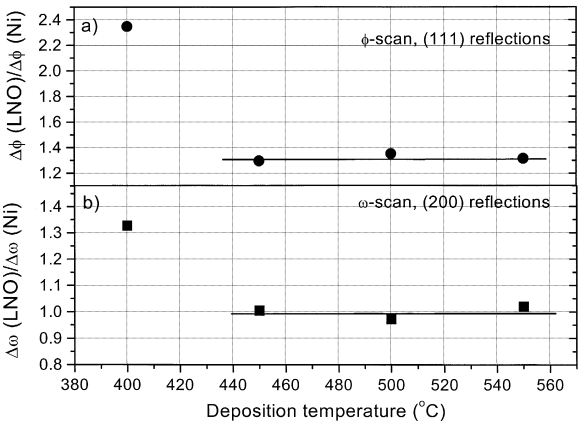

Fig. 2. Dependence of the normalized XRD FWHM peak widths, quantifying the crystallinity of LNO films as a function of deposition temperature. (a) The in-plane distribution width $\Delta\phi$. (b) The out-of-plane distribution width $\Delta\omega$. The lines serve as a visual guide.

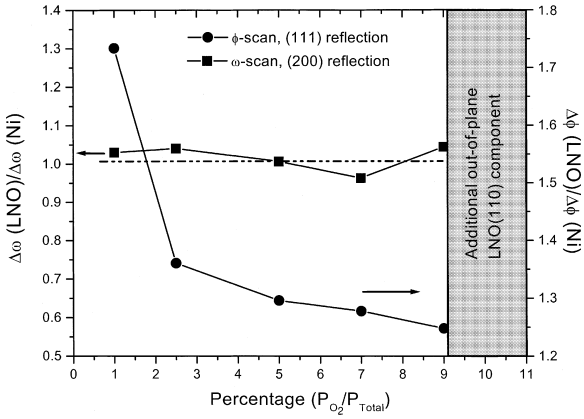

Fig. 3. Effect of O_2 partial pressure on the FWHM ratios of (2 0 0) ω-rocking curves and (1 1 1) ϕ-scans for LNO films on Ni, deposited at 480°C. The dashed lines serve as a visual guide.

significantly affect the crystalline quality of the LNO films. Hence, the combined observations of Figs. 1 and 2 suggest that the optimal range of T_{dep} for epitaxial growth of LNO on Ni should be around 450–500°C. From the experience with other oxides, it is remarkable that well-aligned LNO films can be grown on biaxially textured Ni substrates at temperatures as low as 450°C.

To investigate the influence of the oxygen partial pressure on epitaxial growth of LNO, a series of films were deposited at $T_{dep} = 480$°C in different P_{O_2} values in the range of 0.1–1 mTorr. Fig. 3 plots the ω-rocking curve and ϕ-scan FWHM ratios of LNO and Ni as a function of the percentage of P_{O_2} relative to total sputtering pressure. While P_{O_2} has a positive effect on the in-plane texture of LNO, as evidenced by the substantial decrease in the ϕ-scan FWHM ratios, it does not have a significant affect on the out-of-plane alignment of the films. However, increasing P_{O_2} over a certain limit (>9%) resulted in films having additional components. The latter effect may arise from the formation of interfacial NiO, since we detected the presence of (1 1 1) NiO peak in the XRD θ–2θ spectrum. We speculate that increasing P_{O_2} up to, but not exceeding, 9% during depositions may enhance the crystallinity in LNO by incorporating more O_2 into the lattice. One of the as-deposited LNO films was post annealed in O_2 at 600°C, resulting in a lattice volume reduction of 0.6%. This observation is consistent with previous reports, where a decrease in the lattice parameter was observed with improved oxygen content [12,13]. Such an oxygen-mediated reduction in lattice parameter should improve the lattice match between LNO and Ni, and thus, the in-plane alignment of LNO layers, since biaxially textured cubic Ni has a smaller lattice constant (0.352 nm) than that of pseudo-cubic LNO (0.385 nm).

The epitaxial orientation of the LNO films on textured Ni substrates was characterized by XRD pole figure analysis. A typical (1 1 1) pole figure of a 300 nm thick LNO film, processed at 480°C in 0.5 mTorr P_{O_2}, exhibits a single cube-on-cube epitaxy, as illustrated in Fig. 4. A SEM micrograph of the same LNO film is shown in Fig. 5. Unlike CeO_2 base layers, where crack formation occurs for thicknesses above a few hundred angstroms, LNO layers show a crack-free, smooth, and dense microstructure. Similar surface morphologies were observed for the films deposited at various thicknesses ranging from 50 to 300 nm.

3.2. Growth of YSZ and CeO_2 layers on LNO/Ni substrates

Fig. 6(a) and (b) show the results of XRD θ–2θ scans for the subsequent YSZ films, deposited at

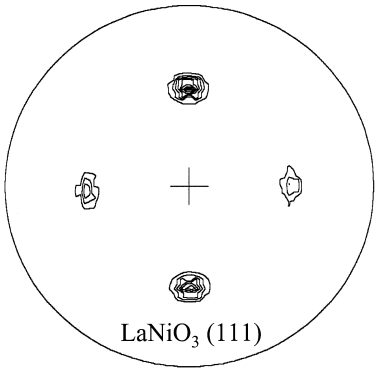

Fig. 4. The (1 1 1) pole figure of a 300 nm thick LNO film deposited on biaxially textured Ni at 480°C. Contour levels are 5, 10, 15, 20, 25, 30, 35, 40.

600°C in 96% Ar + 4% H_2 or in a mixture of 96% Ar + 4% H_2 and O_2, respectively. It is clear that YSZ films grown in reducing atmospheres have a polycrystalline nature (Fig. 6(a)), whereas films deposited under oxidizing conditions have excellent *c*-axis oriented growth (Fig. 6(b)). These results suggest that an adequate level of O_2 is essential to obtain epitaxial growth of YSZ on LNO/Ni substrates. It is likely that this observation is governed more by the underlying LNO layer than by the relatively stable YSZ. That is, under the reducing ambient at 600°C, local degradation may occur in the crystalline quality of the LNO, due to oxygen instability, thereby adversely affecting the

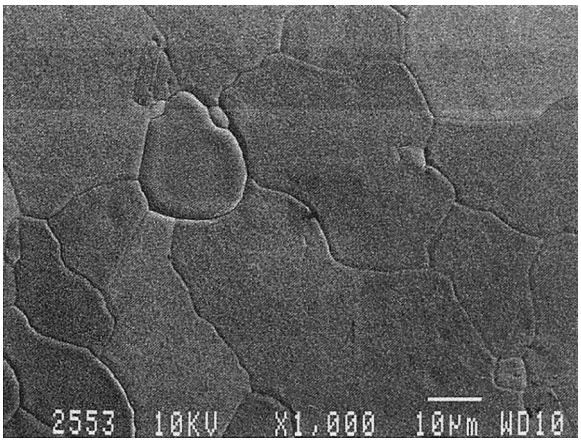

Fig. 5. SEM micrograph of a 300 nm thick LNO film deposited directly on biaxially textured Ni substrate.

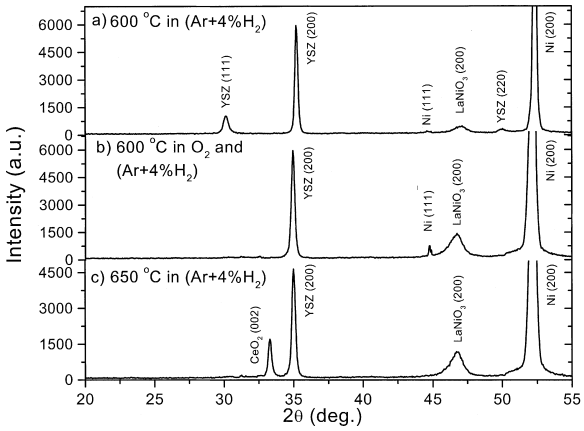

Fig. 6. XRD θ–2θ scans (a) of the YSZ films on LNO/Ni samples processed in 96% Ar + 4% H_2, (b) processed in O_2+(96% Ar + 4% H_2) atmospheres at 600°C and (c) the XRD pattern of the CeO_2/YSZ/LNO/Ni structure, where the top CeO_2 layer was deposited at 650°C in 96% Ar + 4% H_2.

growth of YSZ. The oxidizing environment of Fig. 6(b) assures integrity of both oxides.

Following deposition of YSZ buffer layers, biaxially textured CeO_2 cap layers were grown at 650°C using 10 mTorr of 96% Ar + 4% H_2 atmosphere. This ambient, combined with the system background of water vapor provided sufficient stability for growth of CeO_2. A typical XRD θ–2θ pattern of a CeO_2/YSZ/LNO/Ni structure is shown in Fig. 6(c). The presence of only (0 0 *l*) CeO_2 reflections indicates good out-of-plane texture. The relative in-plane and out-of-plane textures of all the layers are documented in Figs. 7 and 8, respectively. The four-fold symmetry of the ϕ-scan (1 1 1) reflections, shown in Fig. 7, indicates a high degree of in-plane alignment among all layers. The in-plane epitaxial orientations observed in this new buffer-layer architecture are CeO_2[1 1 0]//YSZ[1 1 0]//LNO[1 0 0]//Ni[1 0 0]. The in-plane CeO_2[1 0 0] and YSZ[1 0 0] axes are rotated by 45° with respect to the in-plane LNO[1 0 0] and Ni[1 0 0]. This 45° rotation is anticipated, according to the near-coincidence site lattice theory [14]. The FWHM of the ϕ-scans for Ni(1 1 1), LNO(1 1 1), YSZ(1 1 1) and CeO_2(1 1 1) are 8.9°, 8.9°, 9.6° and 9.5°, respectively, indicating that all the buffer layers closely replicate the in-plane texture of Ni substrates. Out-of-plane

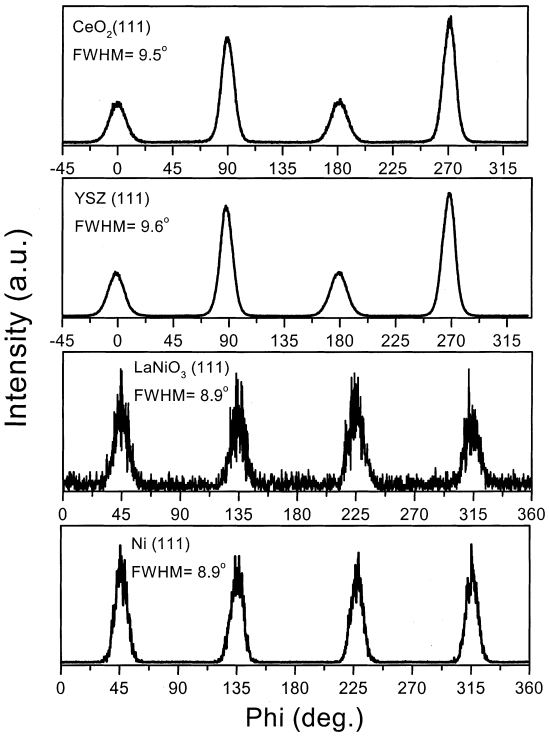

Fig. 7. XRD (1 1 1) ϕ-scans for the CeO_2/YSZ/LNO/Ni structure showing that all buffer layers tend to replicate the in-plane texture of the Ni substrate.

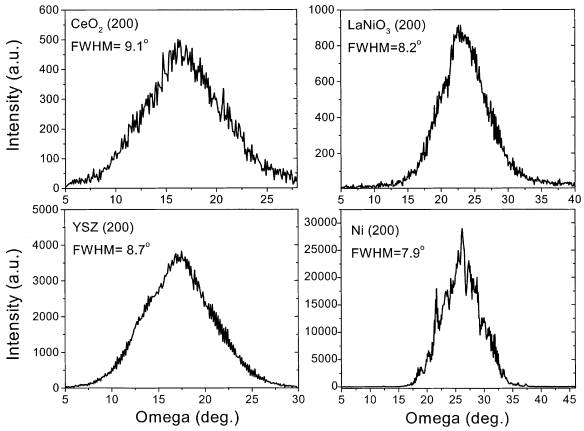

Fig. 8. XRD (2 0 0) ω-rocking curves for the CeO_2/YSZ/LNO/Ni structure showing a good c-axis orientation among all layers.

textures of the buffer layers for the same sample are illustrated in Fig. 8. The FWHM ω-rocking curve scan on the (2 0 0) peak reflections of Ni, LNO, YSZ and CeO_2 are 7.9°, 8.2°, 8.7° and 9.1°, respectively. These results reveal good c-axis alignment among the layers. Thus, from a structural aspect, these XRD characterizations show that CeO_2/YSZ/LNO multilayer buffer structure can be epitaxially grown on biaxially textured Ni substrates.

SEM studies of the completed CeO_2/YSZ/LNO/Ni architecture revealed that the thickness of the base-LNO layer does not have a significant effect on the surface morphology. This point is illustrated in Fig. 9(a) and (b), for samples having 50 and 300 nm thick LNO layers, respectively. Each sample exhibits a homogeneous, featureless and dense surface morphology; only the Ni grain boundaries are apparent. Apparently, LNO base layers as thin as 50 nm can inhibit the formation of NiO during growth in Ni-oxidizing ambients. This is an important feature, since previous work has indicated that NiO tends to diffuse into subsequent buffer layers and presents a potential problem for Ni-based substrates [11,15].

3.3. Results of YBCO films on CeO_2/YSZ/LNO/Ni substrates

The qualifying test for overall suitability of the CeO_2/YSZ/LNO buffer layer structure on Ni is compatible with the YBCO coatings, which were formed at thicknesses of 200 nm. A typical XRD θ–2θ spectrum for a YBCO/CeO_2/YSZ/LNO(50 nm thick)/Ni multilayer structure is shown in Fig. 10. The pattern indicates (0 0 l) reflections only for the YBCO, demonstrating orientation with the YBCO c-axis perpendicular to the substrate surface. The YBCO (1 0 3) pole figure, shown in Fig. 11, indicates a 45° rotated epitaxy, with YBCO[1 0 0]//CeO_2[1 1 0]. The ϕ- and ω-rocking curve FWHM values for the YBCO (1 0 3) and YBCO (0 0 5) reflections are 9.5° and 8.1°, respectively. Both distribution widths are comparable to those of the substrate.

Typical transport J_c data of the YBCO/CeO_2/YSZ/LNO(500 Å thick)/Ni sample, taken at 77 K with the field applied parallel to c-axis, are plotted as a function of applied magnetic field in Fig. 12. The inset of this figure shows the superconducting

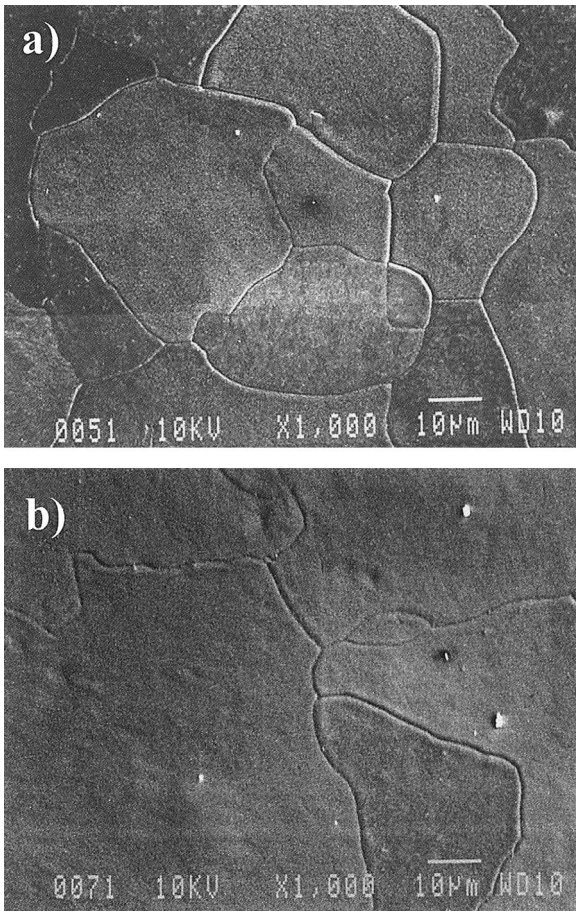

Fig. 9. SEM micrographs of CeO_2/YSZ/LNO/Ni samples having (a) 50 nm and (b) 300 nm thick LNO base layers.

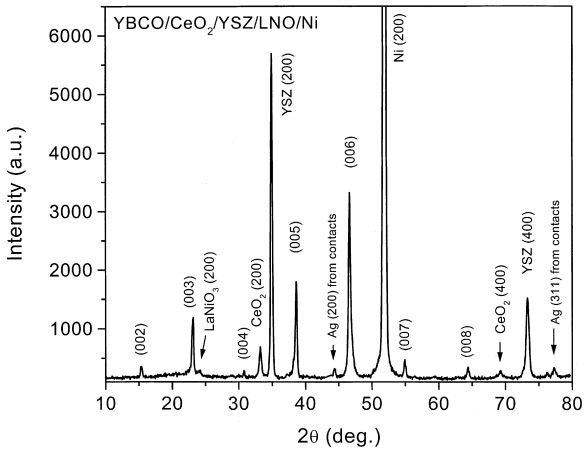

Fig. 10. A typical XRD θ–2θ spectrum for a YBCO film on the CeO_2/YSZ/LNO/Ni multilayer structure. YBCO peaks are labeled by (0 0 *l*) indices. Note the LNO (0 0 2) peak is covered by the YBCO (0 0 6) reflection.

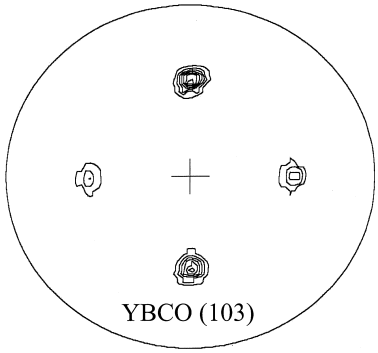

Fig. 11. The (1 0 3) pole figure of YBCO grown on a CeO_2/YSZ/LNO/Ni multilayer. Contour levels are 5, 10, 15, 20, 25, 30, 35, 40.

transition region of the temperature-dependent resistivity, yielding a zero-resistance $T_c = 90.5$ K with a transition width $\Delta T_c \approx 1$ K. Fig. 12 shows a high J_c $(H = 0)$ of 1×10^6 A/cm^2, and an irreversibility field $(H_{irr}) = 8$ T. These values are comparable to those of good YBCO films grown on RABITS having the "standard buffer architecture," CeO_2/YSZ/CeO_2/Ni, and confirm the high-quality epitaxial growth of YBCO on the present, all-sputtered CeO_2/YSZ/LNO/Ni multilayer structure. The J_c and T_c values of several samples studied ranged from 0.75 to 1.3×10^6 A/cm^2, and 88 to 91 K, respectively. As was the case with the structural and morphological observations, the transport properties are largely independent of the LNO base-layer thickness in the range of 50–300 nm.

4. Summary and conclusion

We have demonstrated for the first time, the successful fabrication of high-J_c YBCO coatings on an all-sputter deposited buffer architecture, employing the layer sequence CeO_2/YSZ/LNO/Ni. Due to its significance as a base layer, we have investigated the optimum deposition conditions

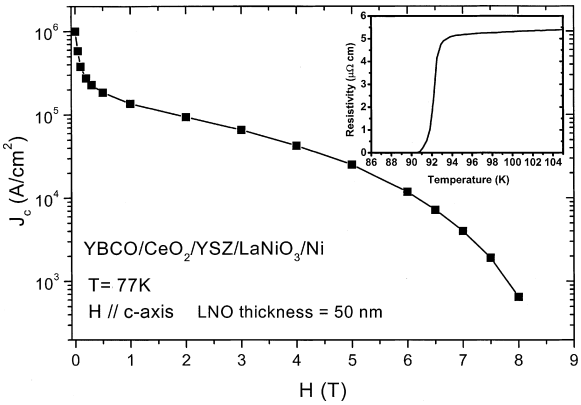

Fig. 12. Magnetic field dependence of J_c of a YBCO/CeO_2/YSZ/LNO/Ni multilayer structure at 77 K. Inset shows the resistive superconducting transition region of the same sample having a 50 nm thick LNO layer. Due to a partial connection between the YBCO and Ni substrate, which occurs through the silver paste and/or silver contacts, the normal state resistivity versus T curve displays a small magnitude and slope.

for the epitaxial growth of LNO on Ni. High quality LNO layers were achieved in oxidizing conditions at temperatures between 450°C and 500°C. In contrast to the out-of-plane texture, the in-plane texture of the LNO layers was found to be sensitive to the oxygen partial pressure during deposition. Unlike CeO_2 base layers, no evidence of thickness dependent crack formation is observed for the LNO layers. Our results indicated that for LNO layer thicknesses in the range 50–300 nm, no noticeable effect was found on the quality of subsequent buffer layers or on the superconducting properties of YBCO coatings. For 200 nm thick YBCO, typical self-field J_c (77 K) values of 1×10^6 A/cm^2 have been achieved. The present results offer additional feasibility for the ultimate development of high-J_c YBCO-coated conductors for power applications of high-temperature superconductivity.

Acknowledgements

Research was co-sponsored by the DOE Division of Materials Sciences, and by the DOE Office of Power Technologies, both under Contract No. DE-AC05-96OR22464 with Lockheed Martin Energy Research Corp. T. Aytug and J.Z. Wu would like to acknowledge NSF Grant No. DMR-9901460 and AFOSR Grant No. F49620-96-1-0358.

References

[1] A. Goyal, D.P. Norton, J.D. Budai, M. Paranthaman, E.D. Specht, D.M. Kroeger, D.K. Christen, Q. He, B. Saffian, F.A. List, D.F. Lee, P.M. Martin, C.E. Klabunde, E. Hatfield, V.K. Sikka, Appl. Phys. Lett. 69 (1996) 1795.
[2] D.P. Norton, A. Goyal, J.D. Budai, D.K. Christen, D.M. Kroeger, E.D. Specht, Q. He, B. Saffian, M. Paranthaman, C.E. Klabunde, D.F. Lee, B.C. Sales, F.A. List, Science 274 (1996) 755.
[3] M. Paranthaman, A. Goyal, F.A. List, E.D. Specht, D.F. Lee, P.M. Martin, Q. He, D.K. Christen, D.P. Norton, J.D. Budai, D.M. Kroeger, Physica C 275 (1997) 266.
[4] J.E. Mathis, A. Goyal, D.F. Lee, F.A. List, M. Paranthaman, D.K. Christen, E.D. Specht, D.M. Kroeger, P.M. Martin, Jpn. J. Appl. Phys. 37 (1998) L1379.
[5] C. Park, D.P. Norton, D.K. Christen, D.T. Verebelyi, R. Feenstra, J.D. Budai, A. Goyal, D.F. Lee, E.D. Specht, D.M. Kroeger, M. Paranthaman, IEEE Trans. Appl. Supercond. 9 (1999) 2276.
[6] F.A. List, A. Goyal, M. Paranthaman, D.P. Norton, E.D. Specht, D.F. Lee, D.M. Kroeger, Physica C 302 (1998) 87.
[7] Q. He, D.K. Christen, J.D. Budai, E.D. Specht, D.F. Lee, A. Goyal, D.P. Norton, M. Paranthaman, F.A. List, D.M. Kroeger, Physica C 275 (1997) 155.
[8] A. Goyal, F.A. List, J. Mathis, M. Paranthaman, E.D. Specht, D.P. Norton, C. Park, D.F. Lee, D.M. Kroeger, D.K. Christen, J.D. Budai, P.M. Martin, J. Supercond. 11 (1998) 481.
[9] S. Oh, J. Yoo, K. Lee, J. Kim, D. Youm, Physica C 308 (1998) 91.
[10] X. Cui, F.A. List, D.M. Kroeger, A. Goyal, D.F. Lee, J.E. Mathis, E.D. Specht, P.M. Martin, R. Feenstra, D.T. Verebelyi, D.K. Christen, M. Paranthaman, Physica C 316 (1999) 27.
[11] Q. He, D.K. Christen, R. Feenstra, D.P. Norton, M. Paranthaman, E.D. Specht, D.F. Lee, A. Goyal, D.M. Kroeger, Physica C 314 (1999) 105.
[12] M. Crespin, P. Levitz, l. Gatineau, J. Chem. Soc. Faraday Trans. 2 79 (1983) 1181.
[13] A. Tiwari, K.P. Rajeev, J. Phys. Condens. Matter 11 (1999) 3291.
[14] R.W. Balluffi, A. Brokman, A.H. King, Acta Metall. 30 (1982) 1453.
[15] C.M. Carlson, J.C. Price, P.A. Parilla, D.S. Ginley, D. Niles, R.D. Blaugher, A. Goyal, M. Paranthaman, D.M. Kroeger, D.K. Christen, Physica C 304 (1998) 82.